Journal of Petroleum Research & Studies

Heat Transfer Analysis in Annular Two Phase Flow Using Finite Difference Method

Basim. O. Hasan
Department of Chemical Engineering, Alnahrain University

Abstract

Heat transfer in two phase flow is widely encountered in oil and gas industry in which heat is transported between two phase the fluid and the pipe wall with a rate depending on the hydrodynamic conditions. In present work, theoretical study was carried out to predict the temperature distribution within the liquid layer in annular gas–liquid (air–water) of two phase flow in presence of heat flux under laminar flow conditions. The temperature distribution was evaluated at different values of liquid Reynolds number (Re_{sL}), gas Reynolds number (Re_{sg}), wall heat flux, and inlet liquid as well as gas temperatures. The finite differences technique was employed to solve the energy equation to obtain the temperature distribution in the liquid layer. Additionally, the effect of Re_{sg} and Re_{sL} on the liquid layer thickness was investigated and discussed. It was found that the presence of heat flux through the pipe wall leads to an increase in the liquid temperature asymptotically with the axial distance (z) depending on the radial distance (r). The maximum increase occurred in the liquid layers adjacent to the pipe surface layers and the minimum increase was at the interface. The fully developed temperature profile varied with radial distance (r) where the surface layers reached at $L_t/d=5$. However, the Lt/d for the layers nearest to the interface was less than 5. At a particular (r) and constant Re_{sg}, the higher the Re_{sL} is, the higher the temperature will be. At a particular Re_{sL} and Re_{sg}, the liquid layer temperature distribution depends largely on the values of applied heat flux and the gas temperature.

Keywords: Two phase, flow, Temperature distribution, finite differences, laminar flow, air-water.

1. Introduction

In oil and gas industry, various flow regimes in two-phase flow pipeline have been encountered depending upon pipeline diameter, the composition of phases and their velocities [1]. Because of the complex nature of the two phase flow, the problem was first approached by empirical methods. The trend has shifted to the modeling approach due to the existence of flow patterns or flow configuration [2]. Annular two–phase flow is characterized by a phase interface separating a thin liquid film from the gas flow in the core region, the presence of a liquid film along the pipe wall and a gas core flowing in the central part of the duct. Despite its apparent simplicity, the annular configuration is very complicated in detail which reflects the great uncertainties in the prediction of the performances of annular two-phase systems. The interface of the film is covered by a complex system of waves, whose behavior is a governing feature. Such waves have different shapes and propagation velocities depend on global flow parameters such as mass flow rates and geometry. The system of waves increases the pressure gradient in the system and gives rise to entrained droplets. In adiabatic flows, droplet concentration, phase velocities, and film shape vary along the pipe until steady values of several hundred diameters downstream of the mixing section are reached. Thus, in two-phase flows, the flow development occurs over much longer distances than in a single-phase flow [3, 4]. Many important questions are still waiting for answers: one of them is related to developing flows structure and interactions. The other crucial question is the physical modeling of two-phase flow [5].

The objective of present study is to analyze and calculate the temperature distributions within the liquid layer adjacent to pipe wall in annular two phase flow conditions (air–water). Moreover, this analyzing has to be achieved in the presence of heat flux through pipe wall at various values of liquid superficial Reynolds number (Re_{sL}), gas superficial Reynolds number (Re_{sg}), inlet liquid and temperatures. Finite difference method is applied to carry out the present analysis.

2. Other Related Works

One of the earliest research works in this field was conducted by Spedding and Nguyen [6] and Chen and Spedding [7]. They developed flow regime maps for Air water two-phase flow through obtaining data at various conditions of vertically downward and vertically upward flow. In the same year, Whalley studied the Air-water flow in a helically coiled tube [8]. On the other hand, Weisman et al, performed an examination of two-phase flow patterns and pressure drop in single and double helically ribbed circular tubes [9]. The authors indicated that swirling annular flow is seen at low qualities once a minimum liquid velocity is exceeded.

Mishima and Hibiki [10] measured the flow regime, void fraction, rise velocity of slug bubbles and frictional pressure loss for air-water flows in capillary tubes. The authors stated that the overall trends of the boundaries between flow regimes were predicted well by Mishima-Ishii's model. The void fraction was correlated well by the drift flux model with a new equation for the distribution parameter as a function of inner diameter. Additionally, the rise velocity of the slug bubbles was also correlated well by the drift flux equation. In the same way, the frictional pressure loss was reproduced well by Chisholm's equation with a new equation for Chisholm's parameter *C* as a function of inner diameter.

Numerous heat transfer coefficient correlations and experimental data for forced convective heat transfer during gas–liquid two-phase flow in vertical and horizontal pipes have been published over the past 40 years [11-13]. Triplett et. al experimentally investigated void fraction and frictional pressure drop of two-phase (air-water) in transparent circular microchannels and in microchannels with semi-triangular [14]. The authors applied a one-dimensional model based on the numerical solution of mass and momentum conservation equations. Moreover, this calculation of test section pressure drop was achieved using various two-phase friction models. For bubbly and slug flow patterns, the two-phase friction factor based on homogeneous mixture assumption provided the best agreement with experimental data. Ide and co-workers illustrated the characteristics of an air–water

isothermal two-phase flow in minichannels [15]. The directions of flow were vertical upward, horizontal and vertical downward. The Authors summarized the characteristics of the flow phenomena in a minichannel with special attention on the flow patterns, the time varying holdup and the pressure loss. The effects of the tube diameters, aspect ratios of the channels on these flow parameters and the flow patterns were investigated. Whereas, Jeong et. al conducted an experimental study on the interfacial area transport (IAT) of vertical, upward, air–water two-phase flows in an annulus channel [16] . The local flow parameters such as void fraction, interfacial area concentration (IAC) and bubble interface velocity were measured at nine radial positions for the three axial locations.

Recently, Wongwises and Pipathattakul [5], Saisorn and Wongwises [17] studied experimentally the characteristics of an adiabatic two-phase air–water flow. They concluded that the void fraction data obtained by image analysis tends to correspond with the homogeneous flow model. Additionally, the two-phase pressure drop is also used to calculate the frictional multiplier. A new correlation of two-phase frictional multiplier is also proposed for practical application.

3. Shear Stresses and Friction Factors

By conducting a force balance on the liquid layer in annular flow, the following equation was obtained [18]:

$$-A_L\left(\frac{dp}{dL}\right)_L - \tau_{wL}S_L + \tau_i S_i = 0 \qquad (1)$$

Rearrange,

$$\left(\frac{dp}{dL}\right)_L = \frac{-(\tau_{wL}S_L - \tau_i S_i)}{A_L} \qquad (2)$$

Where $S_i = \pi d_i L$, $S_L = \pi d L$, A_L is the flow area of the liquid layer and (dP/dL) is the pressure gradient in the liquid layer. The shear stress at the wall (τ_{wL}) and interfacial shear stress (τ_i) are both functions of liquid superficial Reynolds number (Re_{sl}) and gas superficial Reynolds number (Re_{sg}), where:

$$Re_{sl} = \frac{\rho_l u_{sl} d}{\mu_l} \quad (3)$$

$$Re_{sg} = \frac{\rho_g u_{sg} d}{\mu_g} \quad (4)$$

The shear stresses are evaluated as in the case of a single phase flow **[**19**,** 20**]:**

$$\tau_{wL} = f_{wL}\rho_L \frac{u_L^{\,2}}{2} \quad (5)$$

$$\tau_g = f_g \rho_g \frac{u_g^{\,2}}{2} \quad (6)$$

$$\tau_i = f_i \rho_g \frac{(u_g - u_L)^2}{2} \quad (7)$$

Where (u) is the actual average velocity, and (f) is the friction factor which may be expressed in the Blasius form for smooth pipes **[**18, 19,20]**.**

$$f_{wL} = c\left(\frac{d_{hL}\, u_L\, \rho_L}{\mu_L}\right)^{-m} \quad (8a)$$

$$f_g = c\left(\frac{d_{hg}\, u_g\, \rho_g}{\mu_g}\right)^{-m} \quad (8b)$$

For a smooth pipe, (c) is a numerical constant with a value of either 16 or 0.046, and (m) has value of either 1 or 0.2 depending on whether the flow is either laminar or turbulent. The (d_{hL}) is the hydraulic diameter for the liquid phase, being four times the actual flow area over the wetted perimeter **[**20]**.**

The interfacial friction factor (f_i) is one of the key flow parameters and essential in the analysis of two-phase flow [21]. It results from drag exerted by the gas phase on a rough surface, i.e. the rippling liquid phase [22]. Various models are proposed to estimate the interfacial friction factor, f_i. Chun and Kim analyzed and reviewed the interfacial shear stress in two phase air–water flow [21]. They obtained semi-empirical correlation for f_i in stratified wavy flow. However, in the case of annular flow, the assumption of (f_i=f_g) is well-known to be inappropriate. The annular liquid film is supported by a rather complicated system of forces and the liquid surface is always covered with various types of waves [23]. Most of the

existing correlations of (f_i) consist of two parts which are applicable for different flow regimes depending on the flow conditions. The interfacial friction factor or interface roughness is a direct function of the liquid film thickness and Reynolds number [21].

Sripattrapan and Wongwises [35] proposed the following relation for friction factor in two phase flow:

$$f_i = f_g(1+12(\rho_L/\rho_g)^{1/3}(1-\varepsilon^{1/2}) \quad (8c)$$

4. The Void Fraction

The void fraction is defined as **[**12**,** 5**]:**

$$\varepsilon = \frac{V_g}{Vg + V_L} \quad (9)$$

Over the years there were many correlations proposed to predict the void fraction in two phase flow from phase velocity and physical properties. Table (1) lists void fraction models proposed by various authors.

5. Mathematical Analysis

Figure (1) shows a schematic diagram of the annular flow configuration. To find the temperature profile in a liquid layer of thickness (h_L) for a horizontal two-phase annular flow, the following assumptions are adopted:

1- No liquid drops in the gas core and no gas bubbles in the liquid layer.

2- Waves effect at the interface is ignored.

3- The system is hydro-dynamically fully developed, i.e., L/d is large.

4- The air temperature is constant.

5- Physical properties are constant.

6-The thickness of the thermal layer between the liquid layer and gas is less than Δr.

7-Steady state

Table (1) Void fraction correlations proposed by various authors

Author	Correlation
Lokhart and Martinelli [24]	$\varepsilon = \{1+0.28\ (\frac{1-x_f}{x_f})^{0.64}(\frac{\rho_g}{\rho_L})^{0.36}(\frac{\mu_L}{\mu_g})^{0.07}\}^{-1}$, where $x_f = \frac{\dot{m}_g}{\dot{m}_g+\dot{m}_L}$
Fauske [25]	$\varepsilon = \{1+(\frac{1-x_f}{x_f})\ (\frac{\rho_g}{\rho_L})^{0.5}\}^{-1}$
Thom [26]	$\varepsilon = \{1+(\frac{1-x_f}{x_f})(\frac{\rho_g}{\rho L})^{0.89}(\frac{\mu_L}{\mu_g})^{0.18}\}^{-1}$
Braoczy [27]	$\varepsilon = \{1+(\frac{1-x_f}{x_f})^{0.74}(\frac{\rho_g}{\rho L})^{0.65}(\frac{\mu_L}{\mu_g})^{0.13}\}^{-1}$
Zivi [29]	$\varepsilon = \{1+(\frac{1-x_f}{x_f})(\frac{\rho_g}{\rho L})^{2/3}\}^{-1}$, where $x_f = \frac{\dot{m}_g}{\dot{m}_g+\dot{m}_L}$
Chisholm [29]	$\varepsilon = [1+(\frac{1-x_f}{x_f})(\frac{\rho_g}{\rho_L})\ (\frac{\rho_L}{\rho_m})^{0.5}]^{-1}$
Chen and Spedding [18]	$\varepsilon = [1+2.22(\frac{1-x_f}{x_f})^{0.65}(\frac{\rho_g}{\rho_L})^{0.65}]^{-1}$
Chen [7]	$\varepsilon = [1+0.18(\frac{1-x_f}{x_f})^{0.6}(\frac{\rho_g}{\rho_L})^{0.33}(\frac{\mu_L}{\mu_g})^{0.5}]^{-1}$
Hart et al [30]	$1-\varepsilon = \frac{1}{1+\left(\frac{0.005(1+75(1-\varepsilon)}{f_{wL}(1-(1-\varepsilon)^{0.5}}\right)^{0.5}\left[\frac{\rho_g}{\rho_L}\right]^{0.5}\left[\frac{Q_g}{Q_L}\right]^{0.5}}$ $\frac{Q_g}{Q_L} = \frac{u_g A_g}{u_L A_L} = \frac{u_g \varepsilon A}{u_L(1-\varepsilon)A} = \frac{u_{sg}}{u_{sL}}$

The energy equation for fluid flow in pipes is presented as follows [33]

$$\frac{\partial T}{\partial t}+u_r\frac{\partial T}{\partial r}+\frac{u_\theta}{r}\frac{\partial T}{\partial \theta}+u_z\frac{\partial T}{\partial z}=\frac{g}{\rho Cp}+\frac{1}{r}\frac{\partial}{\partial r}(r\alpha\frac{\partial T}{\partial r})+\frac{1}{r^2}\frac{\partial}{\partial \theta}(\alpha\frac{\partial T}{\partial \theta})+\frac{\partial}{\partial z}(\alpha\frac{\partial T}{\partial z}) \quad (10)$$

For liquid layer Equation (10) can be simplifies to give equation (11):

$$u_{zL}\frac{\partial T_L}{\partial z}=\frac{1}{r}\frac{\partial}{\partial r}(r\alpha\frac{\partial T_L}{\partial r})+\alpha(\frac{\partial^2 T_L}{\partial z^2}) \quad (11)$$

The velocity profile is obtained from equation of motion (Navier- Stock equation) [33]:

$$\frac{\partial u_z}{\partial t} + u_r \frac{\partial u_z}{\partial r} + \frac{u_\theta}{r} \frac{\partial u_z}{\partial \theta} + u_z \frac{\partial u_z}{\partial z} = -\frac{1}{\rho} \frac{\partial p}{\partial z} + g_z + \nu \frac{\partial^2 u_z}{\partial r^2} + \frac{\nu}{r} \frac{\partial u_z}{\partial r} + \frac{\nu}{r} \frac{\partial^2 u_z}{\partial \theta^2} + \nu \frac{\partial^2 u_z}{\partial z^2} \quad (12)$$

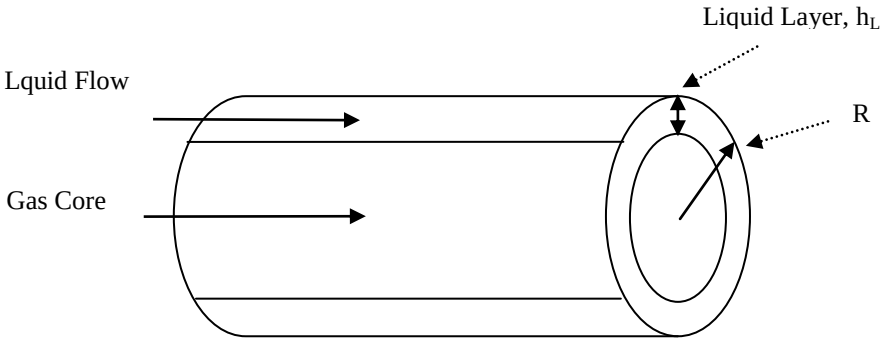

Fig.(1) the annular flow configuration [7].

For liquid layer, equation (12) can be simplified to give equation (13):

$$0 = -\frac{1}{\rho} \frac{\partial p_L}{\partial z} + \nu \frac{\partial^2 u_z}{\partial r^2} + \frac{\nu}{r} \frac{\partial u_z}{\partial r} \quad (13)$$

Equation (13) is solved using the following boundary conditions:

$r = R$, at $u_z = 0$ (14a)

$r = r_i$ at $u_z = u_i$ (14b)

Where (u_i) is the velocity at the interface and (r_i) is the radius at the interface. Therefore, (r_i) is actually the radius of gas core, i.e., it is the distance from the pipe center to the gas-liquid interface. It is a function of void fraction (gas holdup ε) which in turn is function of (u_{sL}) and (u_{sg}). Since $V_g = \pi r_i^2 L$ and $V_g + V_L = \pi R^2 L$, hence equation (9) becomes as follows:

$$\varepsilon = \frac{V_g}{V_T} = \frac{\pi r_i^2}{\pi R^2} \quad (15)$$

Then from Equation (15), the gas core radius is evaluated:

$$r_i = \sqrt{\varepsilon}\ R \quad (16)$$

The liquid layer thickness is then calculated by equation (17):

$$h_L = R - r_i = (1 - \sqrt{\varepsilon})\ R \quad (17)$$

Since (ε) varies with Re_{sL} and Re_{sg}, then h_L becomes a function of Re_{sL} and Re_{sg}. It is known that the hydraulic diameter (d_{hL}) is equal to 4 times (Flow area/wetted perimeter):

$$d_{hL} = \frac{4\ (1-\varepsilon)\ \frac{\pi}{4}\ d^2}{\pi\ d} = (1-\varepsilon)\ d \qquad (18)$$

Where (1-ε) represents the liquid holdup. Equation (13) can be rearranged as follows:

$$\frac{\partial}{\partial r}\left(r\frac{\partial u_{zL}}{\partial r}\right) = \left(\frac{1}{\mu}\frac{\partial p_L}{\partial z}\right)r \qquad (19)$$

The integration of equation (13) yields the following equation:

$$u_{zL} = \frac{\Delta P/L}{4\mu} r^2 + c_1 \ln r + c_2 \qquad (20)$$

By applying the boundary conditions (14), the velocity profile in the liquid layer can be correlated as follows:

$$u_{zL} = \frac{\Delta P}{4L\mu}(r^2 - R^2) + \left[\frac{\Delta P}{4L\mu}(R^2 - r_i^2) + u_i\right]\frac{\ln\frac{r}{R}}{\ln\frac{r_i}{R}} \qquad (21)$$

Now Equation (21) is substituted in Equation (11) to obtain the following expression:

$$\left\{\frac{\Delta P}{4L\mu}(r^2 - R^2) + \left[\frac{\Delta P}{4L\mu}(R^2 - r_i^2) + u_i\right]\frac{\ln\frac{r}{R}}{\ln\frac{r_i}{R}}\right\}\frac{\partial T_L}{\partial z} = \frac{1}{r}\frac{\partial}{\partial r}\left(r\alpha\frac{\partial T_L}{\partial r}\right) + \alpha\left(\frac{\partial^2 T_L}{\partial z^2}\right) \qquad (22)$$

Then Equation (22) is solved using the finite difference method to obtain the temperature profile axially and radially in the liquid layer, i.e, T = f (z, r). The boundary conditions used to solve Equation (22) are as follows:

$T = T_{Lo}$	at	Z = 0	(23a)
T = finite	at	Z = L	(23b)
$q = q_w$	at	r = R	(23c)
$T = T_i$	at	$r = r_i$	(23d)

T_{Lo} is the liquid inlet temperature. The conduction in the direction of flow ($\frac{\partial^2 T}{\partial z^2}$) is low compared to convection term (u_z dT/dz) and thus it can be ignored. The pressure drop in Equation (22) is obtained from Equation (2). The shear stress is defined as [30]:

$$\tau_i = f_i \frac{\rho_L (u_g - u_L)^2}{2} \quad (24)$$

and the liquid area is calculated as:

$$A_L = \pi(R^2 - r_i^2) \quad (25)$$

For annular flow, Dukler et al [40] showed that:

$$\tau_i = \tau_w \varepsilon^{0.5} \quad (26)$$

and for laminar flow the following expression is valid [5, 19,]:

$$f_{wL} = \frac{16}{\mathrm{Re}_{sL}} \quad (27)$$

At the interface, the friction velocity is given by [34]:

$$u_i^* = u_i \sqrt{\frac{f_i}{2}} = \sqrt{\frac{\tau_i}{\rho_g}} \quad (28)$$

Hence from Equations (5), (26), and (28), the following expression obtained:

$$u_i = \sqrt{\frac{f_{wL}\rho_L}{f_i \rho_g}} \varepsilon^{1/2} u_L \quad (29)$$

The liquid layer is divided in to nodes from liquid-gas interface to the liquid wall. Figure (2, 3) showes all 30 nodes spread throughout the liquid layer and the numerical notations for the nodes.

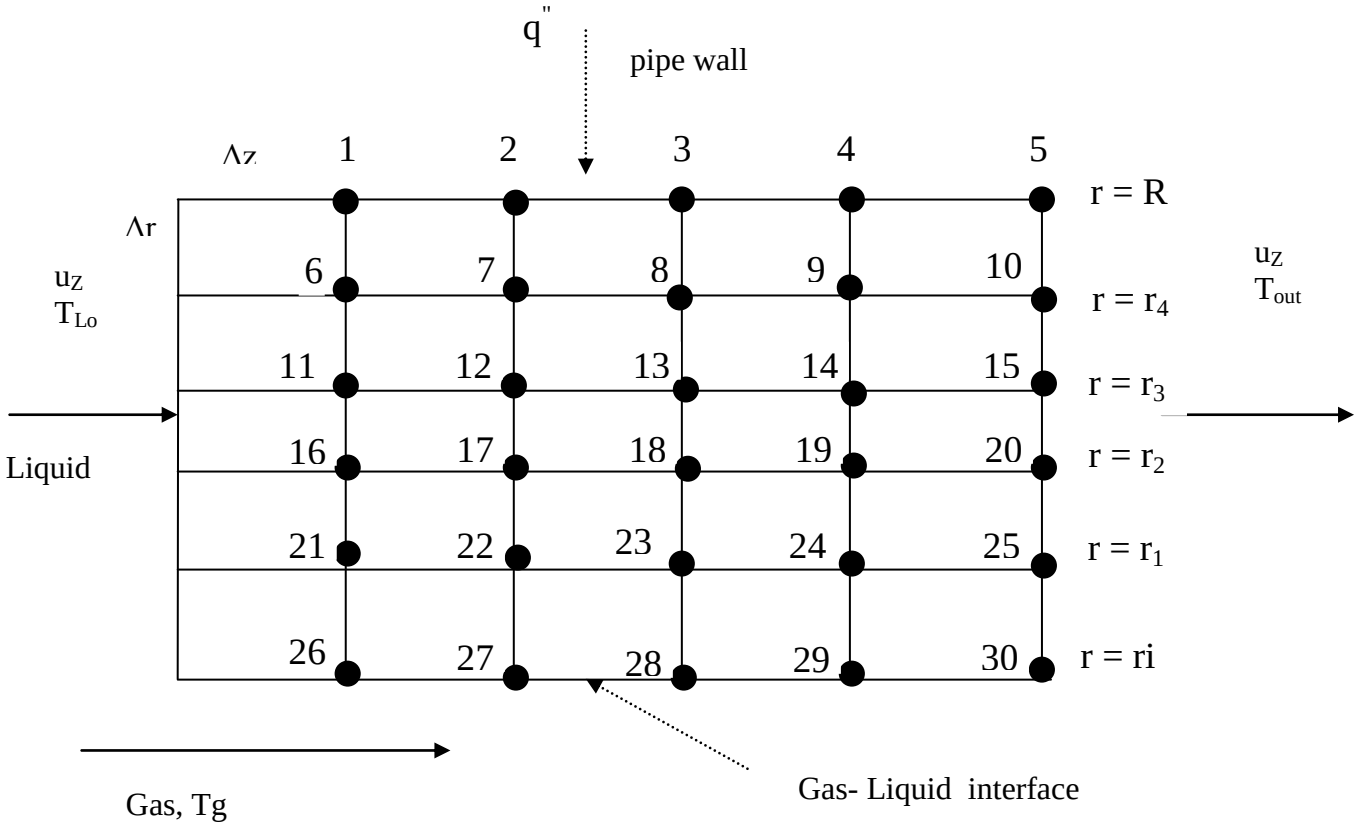

Fig.(2) Liquid layer Divided into 30 nodes Nodes.

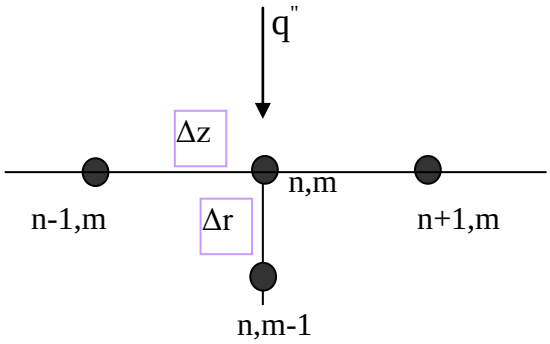

Fig.(3) Surface Nodes.

To find the temperature distribution in the liquid layer, Equation (22) is solved by using finite difference method. The liquid layer divided into 6 nodes radially and 5 nodes axially (total 30) as shown in Figure 2. The radial increment is $\Delta r=(R-r_i)/6$

and the axial increment is Δz= L/5. Calculations are performed for 1 m length and 0.1 m diameter. The temperatures of nodes 6 to 30 are obeying Equation (22), while the temperatures of nodes adjacent to the surface where the velocity is zero. Nodes 1 to 6 are determined from energy balance on each node. For surface nodes performing heat balance on nodes (n, m) yields:

$$k_L A_z \frac{T_{n-1,m} - T_{n.m}}{\Delta z} + k_L A_Z \frac{T_{n+1,m} - T_{n.m}}{\Delta z} + k_L A_r \frac{T_{n,m-1} - T_{n.m}}{\Delta r} + q'' A_r = 0 \quad (30)$$

Rearranging

$$T_{n-1,m} + T_{n+1,m} - 2T_{n.m} + \frac{A_r \Delta z}{A_z \Delta r}(T_{n,m-1} - T_{n.m}) + q'' \frac{A_r \Delta z}{A_z} = 0 \quad (31)$$

For surface nodes (1 to 4 except 5) the cross sectional area (A_z) for each node is

$$A_z=\pi[R^2-(r_4+\Delta r/2)^2] \quad (32)$$

The surface area for each node (except node 5) is

$$A_r = 2\pi(r_4 + \frac{\Delta r}{2})\Delta z \quad (33)$$

For node 5 (half a node)

$$A_r = 2\pi(r_4 + \frac{\Delta r}{2})\frac{\Delta z}{2} \quad (34a)$$

For nodes other than surface nodes

$$A_z=\pi(r_{n+1}{}^2-r_n{}^2)(0.2) \quad (34b)$$

$$A_r=2\pi(r_n$$

he position of node, hence

$$+\Delta r/2)(0.2) \quad (34c)$$

where n denotes t node 1

$$T_o + T_2 - (2 + \frac{A_r \Delta z}{A_z \Delta r})T_1 + \frac{A_r \Delta z}{A_z \Delta r} T_6 + q'' \frac{A_r \Delta z}{A_z} = 0 \quad (35)$$

where T_o is the liquid inlet temperature (T_{Lo}).

node 2

$$T_1 + T_3 - (2 + \frac{A_r \Delta z}{A_z \Delta r})T_2 + \frac{A_r \Delta z}{A_z \Delta r} T_7 + q'' \frac{A_r \Delta z}{A_z} = 0 \quad (36)$$

node 3

$$T_2 + T_4 - (2 + \frac{A_r \Delta z}{A_z \Delta r})T_3 + \frac{A_r \Delta z}{A_z \Delta r} T_8 + q'' \frac{A_r \Delta z}{A_z} = 0 \quad (37)$$

node 4

$$T_3 + T_5 - (2 + \frac{A_r \Delta z}{A_z \Delta r})T_4 + \frac{A_r \Delta z}{A_z \Delta r} T_9 + q'' \frac{A_r \Delta z}{A_z} = 0 \quad (38)$$

node 5

$$k_L A_z \frac{T_{n-1,m} - T_{n.m}}{\Delta z} + + k_L \frac{A_r}{2} \frac{T_{n,m-1} - T_{n.m}}{\Delta r} + q'' \frac{A_r}{2} = 0$$

or

$$T_4 + (1 + \frac{A_r \Delta z}{2A_z \Delta r})T_5 + \frac{A_r \Delta z}{2A_z \Delta r} T_{10} + q'' \frac{A_r \Delta z}{A_z} = 0 \quad (39)$$

For nodes 6 to 30, Equation (22) holds. Writing equation (22) in terms of finite difference form:

$$\frac{\partial T}{\partial z} = \frac{T_{n,m} - T_{n-1,m}}{\Delta z} \quad (40)$$

$$\frac{\partial T}{\partial r} = \frac{1}{2}\left(\frac{T_{n,m+1} - T_{n,m}}{\Delta r} + \frac{T_{n,m} - T_{n,m-1}}{\Delta r}\right) = \frac{T_{n,m+1} - T_{n,m-1}}{2\Delta r} \quad (41)$$

$$\frac{\partial^2 T}{\partial r^2} = \frac{T_{n,m+1} + T_{n,m-1} - 2T_{n,m}}{(\Delta r)^2} \quad (42)$$

$$\left\{\frac{\Delta P}{4L\mu}(r_n^2 - R^2) + \left[\frac{\Delta P}{4L\mu}(R^2 - r_i^2) + u_i\right]\frac{\ln\frac{r_n}{R}}{\ln\frac{r_i}{R}}\right\}\frac{T_{n,m} - T_{n-1,m}}{\Delta z} = \alpha\left(\frac{T_{n,m+1} + T_{n,m-1} - 2T_{n,m}}{(\Delta r)^2} + \frac{1}{r_n}\frac{T_{n,m+1} - T_{n,m-1}}{2\Delta r}\right) \quad (43)$$

Where, $\Delta r = h_L/5$, and $\Delta z = L/5$. T_g is the inlet gas temperature which is considered to be constant.

5.1 Steps of Calculations

The calculations are performed for 1 m length and 0.1 m diameter of a horizontal tube. The following steps are used to fulfill the requirements to solve the proposed system:

1- For particular Re_{sL} and Re_{sg}, the (ε) is calculated using chisholm model (29) available in Table 2.

2- r_i from Equation (16) and(h_L) is calculated using equation (17).

3- $\Delta r=(R-r_i)/6$ and $\Delta z=L/5=0.2$ m.

4- A_r and A_z are calculated for each node.

5- u_i is calculated from Eq. (29) with f_{wL} from equation. (5) and f_i from Sripattrapan and Wongwises model [35].

6- τ_i is calculated from Equation. (7)

7- A_L is calculated using Equation (25) with $S_i=\pi d_i L$ and $S_L=\pi dL$.

8- dP/dL is calculated via Equation (2).

9- u_i and r_i are substituted in nodes 6 to 30.

10- Specify the values of (q_w) and the input liquid temperature (T_{Lo}) and gas temperature (T_g) and the physical properties for liquid and gas.

11- All the above variables are substituted in nodal equations. These nodal equations are solved using iteration method employing personal computer.

The calculations are carried out at different values of Re_{sL}, Re_{sg}, inlet liquid temperature (T_{Lo}), gas temperature T_g, and wall heat flux.

6. Results and Discussion

In the 30 nodes, two sets of equations were implemented. The first set of equations is for nodes (1) to (5) and the second set of equations are for nodes (6) to (30). These equations contain 30 unknown temperatures. These equations were solved using iteration method by assuming initial values of temperatures and new values were found until the values converge to constant temperature. A computer program was employed to perform the iteration. The results were plotted in Figures 4 to 16.

Figure 4 shows the variation of gas core radius (r_i) with Re_{sL} at various Re_{sg}. It was developed using equation (16) with (ε) from Chisholm model [29]. The Figure shows that as (Re_{sL}) increases, (r_i) decreases by increasing thickness of

liquid layer, (h_L) as evident by figure 5. Moreover, figures (4- 5) indicate that the increase in (Re_{sg}) leads to an increase in (r_i) and decrease in (h_L) respectively. Figures (6- 9) show the variation of temperatures with axial distance (z/L) at different radial distance (r). These Figures reveal that the temperature increases with increasing (z) and (r). At the first 0.2 m from applying heat flux, the temperature increased considerably. This increase depends on (r), i.e. the higher the r is, the higher the temperature will be. The lowest increase took place in the interface nodes (where $r = r_i$) because of the effect of gas temperature while the highest increase was in the surface nodes (where r = R) because of the effect of heat flux through the wall. Moreover, these figures indicate that the nodes located at the surface have high temperatures because the presence of heat flux. When (r) decreases (as the interface is approached) the temperature decreases towards the gas temperature. Figure (6) shows that the temperature at the surface (r=5 cm) reaches 17 ^oC while the temperature at the interface (r=4.9 cm) is slightly higher than that of gas (10 ^oC). Figure 7 shows how the gas temperature affects the nodal temperature especially the temperature of the nodes at the interface and the adjacent nodes. The gas temperature shifts the nodal temperature towards it. Generally, the surface temperatures are greatly affected by the wall heat flux through the wall and slightly by gas temperature; however, the interface temperatures are greatly affected by gas temperature and slightly by the wall heat flux.

Figures (10-11) show the effect of (Re_{sL}) on the temperature profile for surface nodes of (Re_{sg}=7000) and different values of T_{Lo} and T_g. These Figures reveal that as (Re) decreases, the temperature of surface nodes decreases. This trend is interpreted as follows: the values of temperature at the surface nodes are affected by the values of interface temperature which are in turn affected by the gas temperature. When (Re_{sL}) decreases, the thickness of liquid layer decreases leading to decrease in the thickness of the thermal layer in the wall vicinity according to [36]:

$$\delta = 25 Re_{sL}^{-7/8} h_L \quad (44)$$

This thermal layer represents the main resistance to heat transfer in the liquid between the liquid and pipe surface [37, 38, 39]. Once the (δ) decreases, the heat transfer between the pipe wall and interface increases leading to shift in the temperature at the wall towards the interface temperature (or gas temperature). The decrease of temperature with (z/L) in Figure 11 is sharper than the decrease in Figure 10 because the gas temperature is lower in the former. Figures 12 and 13 show the effect of the wall heat flux on the surface nodes temperature. It is evident that the higher the heat flux is, the higher is the temperature. This trend holds at each radial distance (r). Generally, at a particular (Re_{sL} and Re_{sg}) the presence of heat flux increases the nodes temperature but this increase depends on (r) and (T_g). Figure 14 indicates that the higher the inlet liquid temperature is, the higher is the nodal temperature. In the same manner, the same behavior appears at Figure 15 where as the gas (Re) increases, the temperature profile increases too. Figure 16 shows the effect of gas temperature on the temperature of the surface nodes. It is clear that as the gas temperature increases, temperature of surface nodes increases.

7. Conclusion

The proposed two phase flow is considered highly nonlinear system. Therefore, seeking an analytical solution is a quit difficult task. The present is work is an attempt to solve system numerically and to obtain the temperature distribution for the liquid layer of air-water system. The finite difference method gave the capability of evaluating distribution of temperature within the liquid layer radially and axially for wide range of (Re), heat flux, liquid inlet temperature, and gas temperature. This technique is an efficient way for predicting the temperature distribution and could be employed to solve all types of two phase flow patterns. However, it needs an appropriate relations for momentum transfer parameters such

as shear stress, friction factor, and void fraction to give an accurate results. The presence heat flux through pipe wall led to an increase in the temperature within the liquid layer axially and radially. The maximum increase occurs in liquid layers adjacent to the pipe surface layers and the minimum increase is at the interface because of the effect of gas temperature. As a result, when (Re_{sL}) decreases, the temperature of surface nodes decreases as well. As the inlet liquid and gas temperatures increase, the temperature of surface also increases.

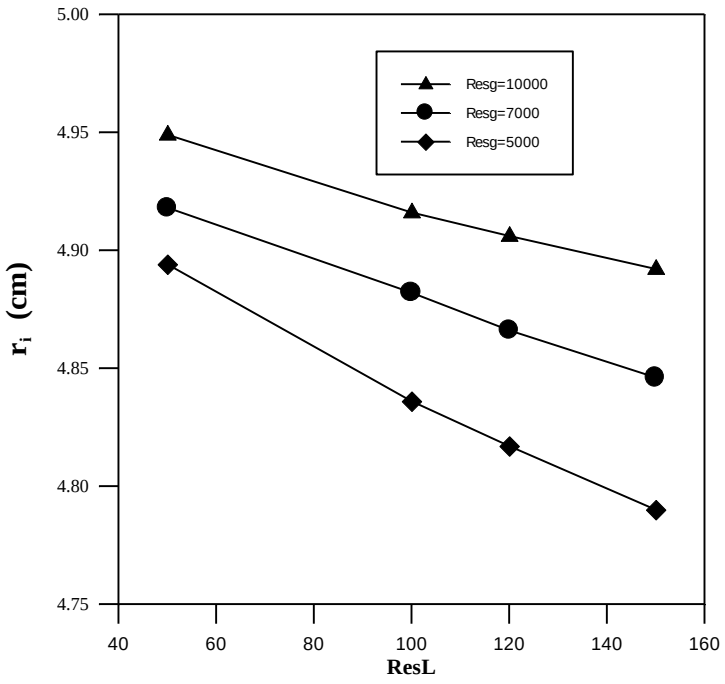

Fig.(4) Effect of Re_{sL} and Re_{sg} on Gas Core Radius (r_i).

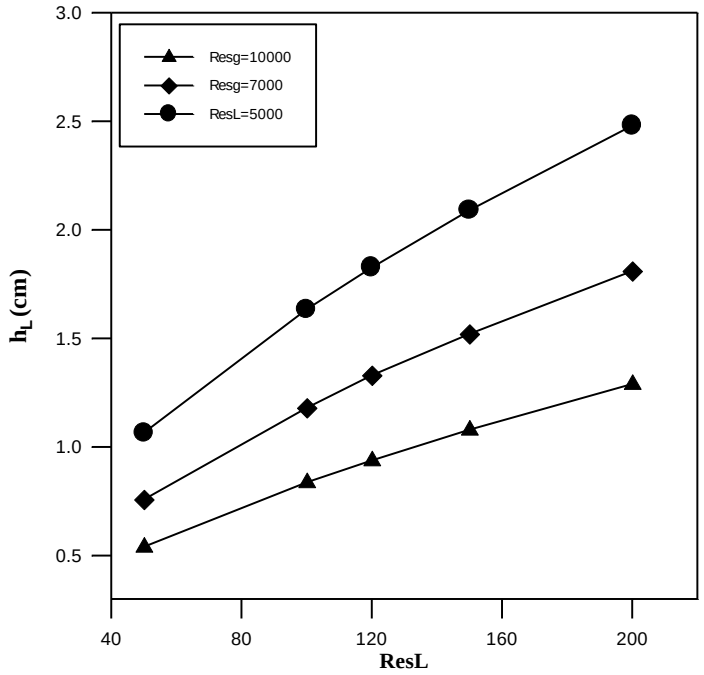

Fig. (5) Variation of Liquid Layer Thickness with Re_{sL} at various Re_{sg}.

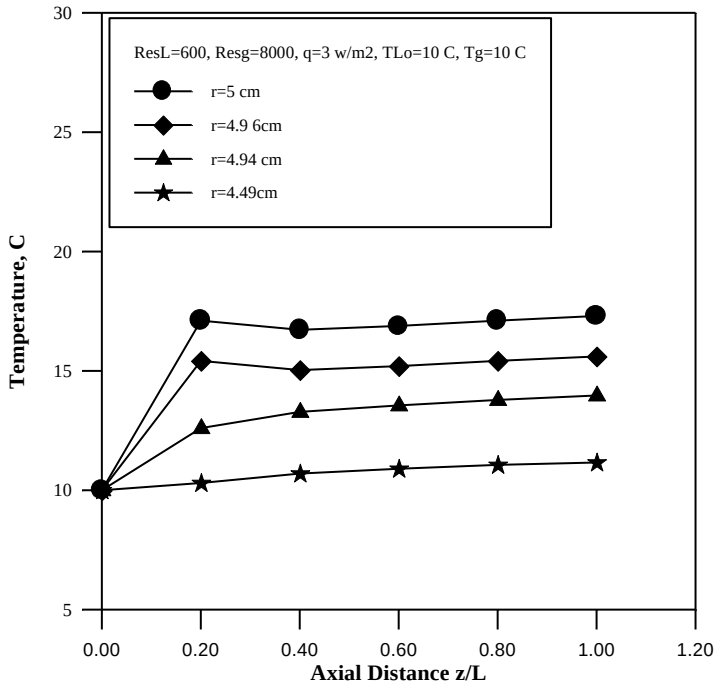

Fig. (6) Variation of temperature with axial distance at various radial distances with T_{Lo}=10 ^oC and T_g=10 ^oC.

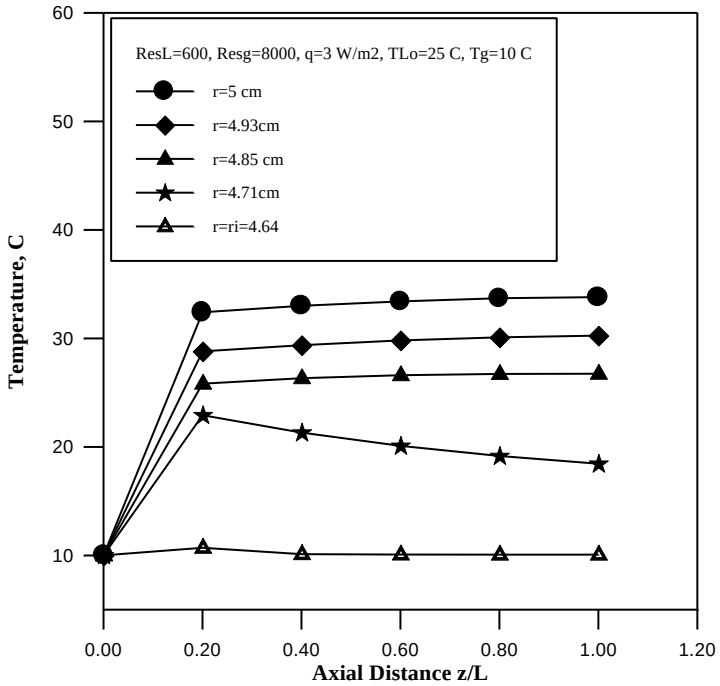

Fig. (7) Variation of temperature with axial distance at various radial distances with T_{Lo}=10 ^{o}C and T_{g}=10 ^{o}C.

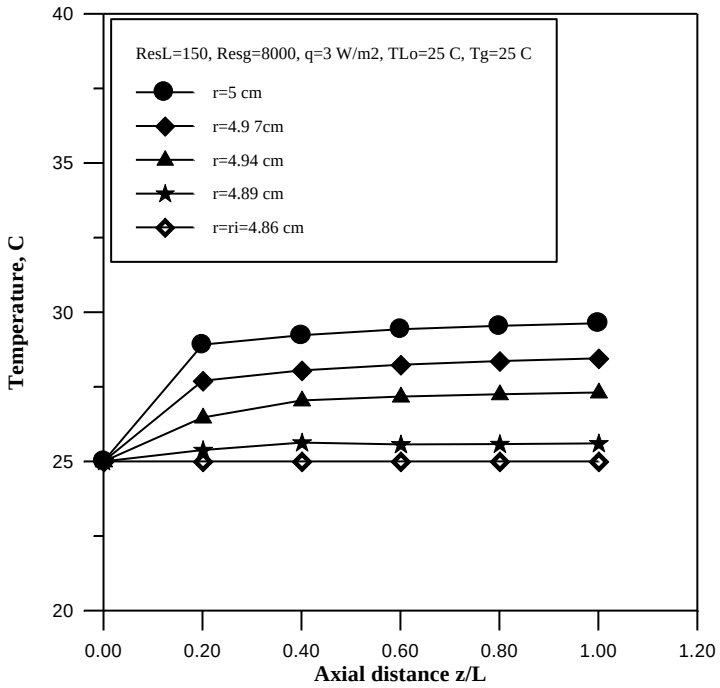

Fig. (8) Variation of temperature with axial distance at various radial distances for Re_{sL}=150, T_{Lo}=25 ^{o}C and T_{g}=25 ^{o}C.

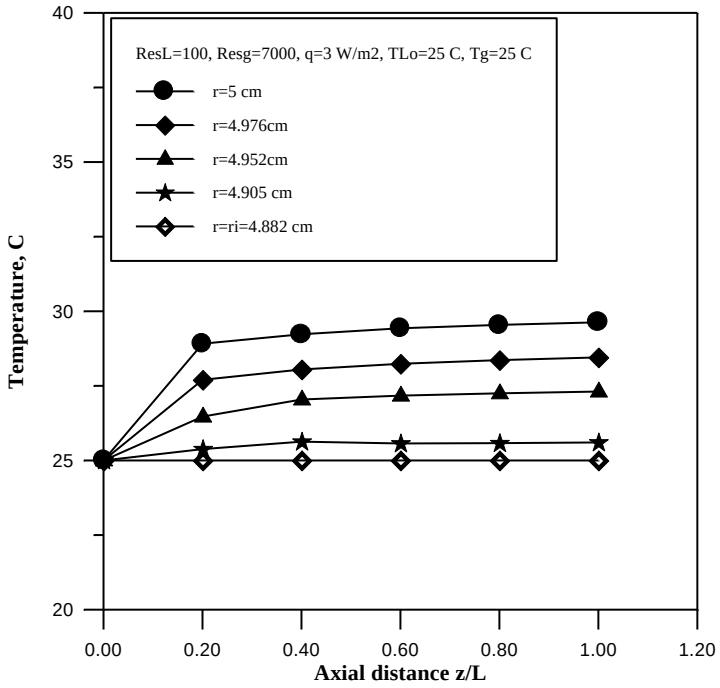

Fig. (9) Variation of temperature with axial distance at various radial distances for Re_{sL}=100, T_{Lo}=25 ^{o}C, and T_g=25 ^{o}C.

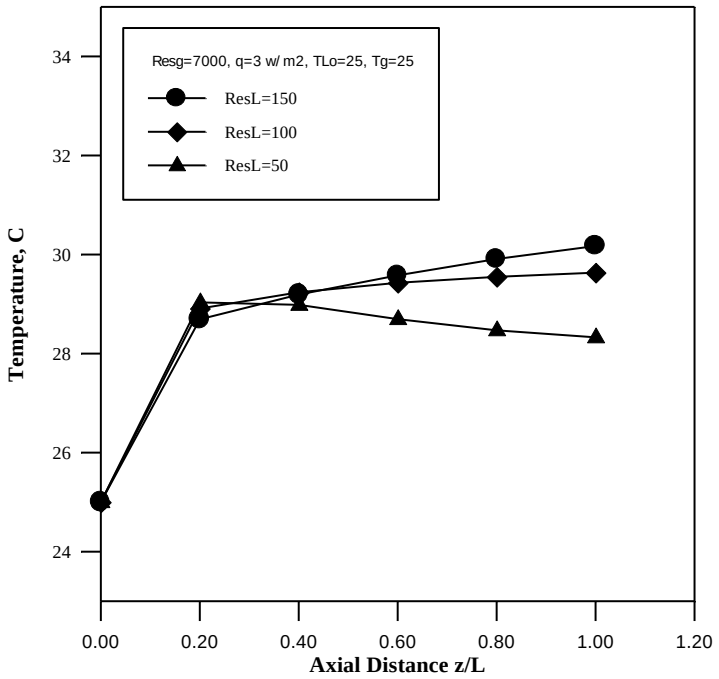

Fig. (10) Variation of surface temperature with axial distance at various Re_{sL}.

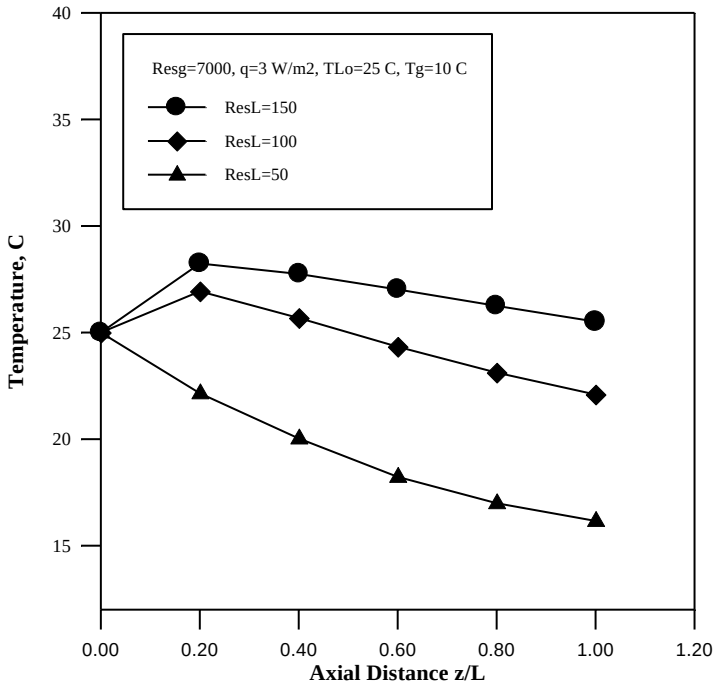

Fig. (11) Variation of surface temperature with axial distance at various Re_{sL}.

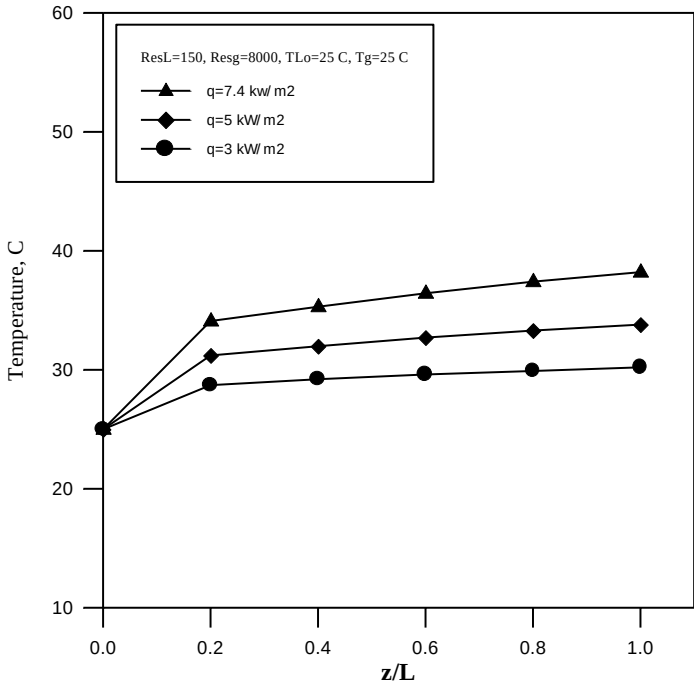

Fig. (12) Effect of heat flux on the surface temperature profile.

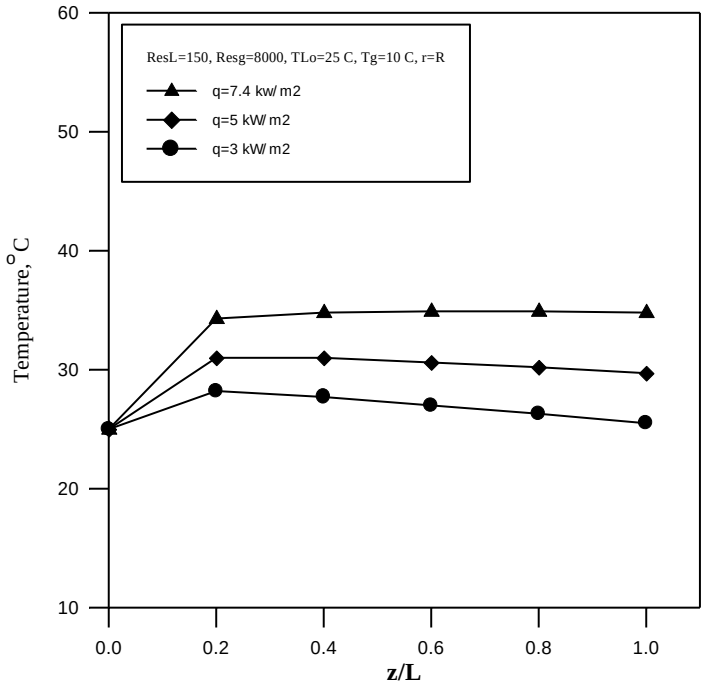

Fig. (13) Effect of heat flux on the temperature profile.

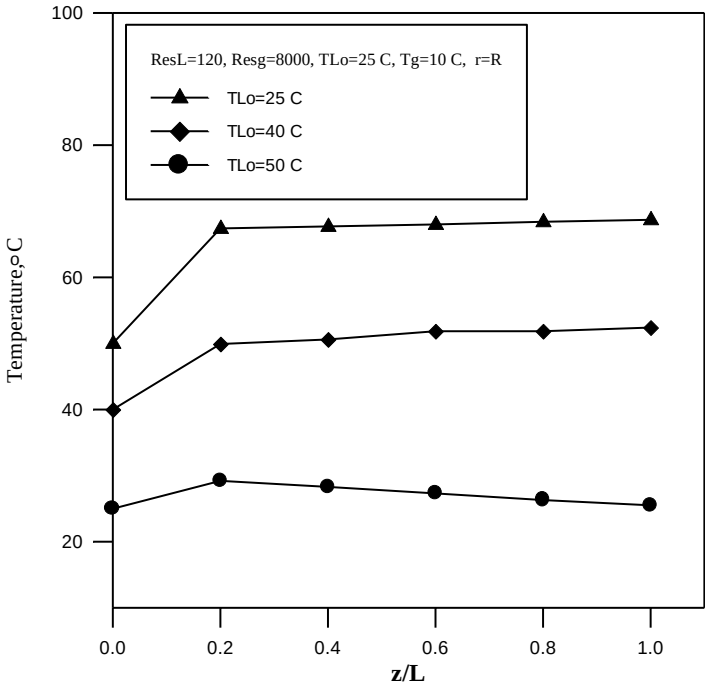

Fig. (14) Effect of inlet liquid temperature on the temperature profile in the surface layers

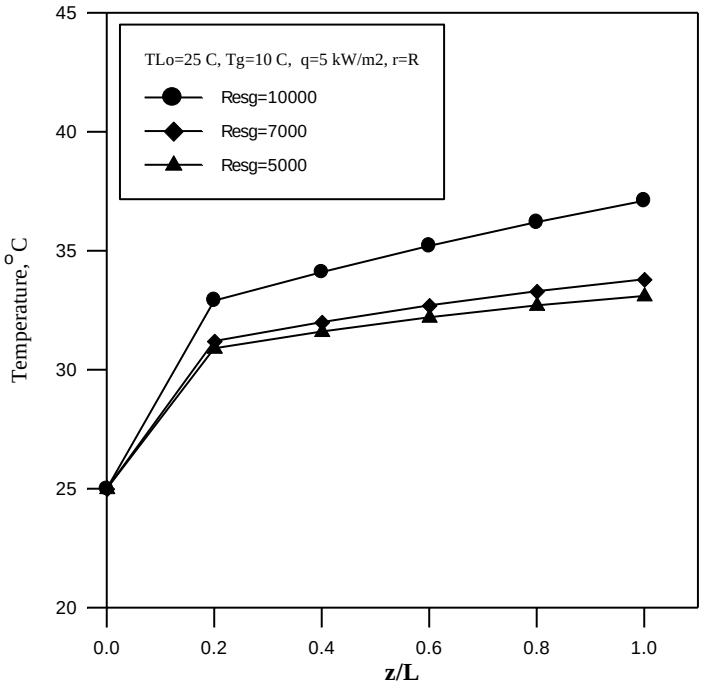

Fig. (15) Effect of Re of gas on the temperature profile in the surface layer

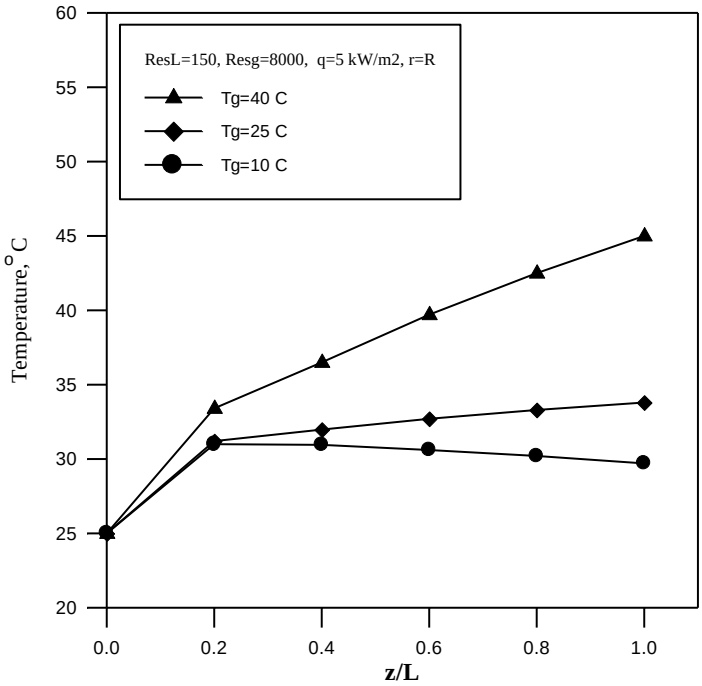

Fig. (16) Effect of gas temperature on the surface nodes temperature.

7. References:

1. Mishima K. and Hibiki T., 1996, Some characteristics of air-water two-phase flow in small diameter vertical tubes, International Journal of Multiphase Flow, Volume 22, Issue 4, P. 703-712.
2. Ansari M., D. Sylvister, C. Sariea, O. Shahom, and J. P. Brill, 1994, " Comprehensive Mechanistic Model for Upward Two Phase Flow in Well Bores", SPE, Production and Facilities, May, P. 143-151.
3. Fossa M., Pisoni C. and Tagliafico L., 1995, Experimental direct contact heat tranfser in upward air-water developing annular flow, International Communications in Heat and Mass Transfer, Volume 22, Issue 6, P. 825-835.
4. Fossa, M., 1995, " A Simple Model to Evaluate Direct Contact Heat Transfer and Flow Characteristics in Annular Two Phase Flow", In. J. Heat and Fluid Flow, 16, P. 272-279.
5. Wongwises S. and Pipathattakul M., 2006, Flow pattern, pressure drop and void fraction of two-phase gas–liquid flow in an inclined narrow annular channel, Experimental Thermal and Fluid Science, Volume 30, Issue 4, P. 345-354.
6. Spedding P. L. and Nguyen V. T., 1980, Regime maps for air water two phase flow Chemical Engineering Science, Volume 35, Issue 4, P. 779-793.
7. Chen, J.J.J., 1986. A further examination of void-fraction in annular two-phase flow. Int. J. Heat Mass Transfer 29, P. 1760–1763.
8. Whalley P. B., 1980, Air-water two-phase flow in a helically coiled tube, International Journal of Multiphase Flow, Volume 6, Issue 4, Pages 345-356.
9. Weisman J., Lan J. and Disimile P, 1994, Two-phase (air-water) flow patterns and pressure drop in the presence of helical wire ribs, International Journal of Multiphase Flow, Volume 20, Issue 5, P. 885-899.
10. Kawahara A., Chung P. M. and Kawaji M., 2002, Investigation of two-phase flow pattern, void fraction and pressure drop in a microchannel, International Journal of Multiphase Flow, Volume 28, Issue 9, P. 1411-1435.

11. Kim, D., Ghajar, A.J., Dougherty, R.L., Ryali, V.K., 1999. Comparison of 20 two-phase heat transfer correlations with seven sets of experimental data, including .ow pattern and tube inclination e.ects. Heat Transfer Eng. 20, 15–40.

12. Kim D., and Ghajar A., 2002, Heat Transfer Measurements and Correlations for Air- Water Flow patterns in Horizontal Pipe, Experimental Thermal and Fluid Science J., 25, P. 659-676.

13. Kim J. and Ghajar, A.J., (2006), A general heat transfer correlation for non-boiling gas–liquid flow with different flow patterns in horizontal pipes, International Journal of Multiphase Flow 32, 447–465

14. Ide H., Kariyasaki A. and Fukano T., 2007, Fundamental data on the gas–liquid two-phase flow in minichannels, International Journal of Thermal Sciences, Volume 46, Issue 6, P. 519-530.

15. Jeong J. J., Ozar B., Dixit A., Juliá J.E, Hibiki T. and Ishii M., 2008, Interfacial area transport of vertical upward air–water two-phase flow in an annulus channel, International Journal of Heat and Fluid Flow, Volume 29, Issue 1, Pages 178-193.

16. Saisorn S. and Wongwises S., 2008, A review of two-phase gas–liquid adiabatic flow characteristics in micro-channels, Renewable and Sustainable Energy Reviews, Volume 12, Issue 3, P. 824-838.

17. Chen J.J. and P.L. Spedding, 1983 " An Analysis of Holdup in Horizontal Two Phase Gas-|Liquid Flow" Int. J. Multiphase Flow, Vol.9,No. 2, P.147-159.

18. Taitel Y. and Dulker, A.E.,1976, A model for predicting flow regime transitions in horizontal and near horizontal gas-liquid flow. AIChE.JI,Vol.22.P-47-55.

19. Wongwises, S. and P. Naphon, 2000, "Heat transfer and flow characteristics in vertical annular two phase two component flow" Thammasat. Int. J. Sc. Tech. Vol.5, No. 1, January.

20. Chun, M. H. and Y. S. Kim, 1995,"A Semi empirical correlation for adiabatic interfacial friction factor in horizontal air water countercurrent stratified flow", Int. Comm. Heat Mass Transfer, Vol. 22,No. 5, P. 617-628.
21. Eck B., 1973, Technische Stromunglehre, Springer, New York.
22. Butterworth D., Air-water annular flow in a horizontal tube, 1972, Prog. Heat Mass Transfer , Vol.6 ,P-235-251.
23. Lockhart, R.W., Martinelli, R.C., 1949. Proposed correlation of data for isothermal two-phase, two component flow in pipes. Chem. Eng.Progr. 45, 39–48.
24. Fauske, H., 1961. Critical two-phase, steam–water flows. In: Proceedings of the Heat Transfer and Fluid Mechanics Institute. Stanford University Press, Stanford, CA, P. 79–89.
25. Thom, J.R.S., 1964. Prediction of pressure drop during forced circulation boiling of water. Int. J. Heat Mass Transfer 7, P. 709–724.
26. Baroczy, C.J., 1966. A systemic correlation for two phase pressure drop. Chem. Eng. Progr. Symp. Ser. 62, P. 232–249.
27. Zivi, S.M., 1964. Estimation of steady state steam void fraction by means of the principle of minimum entropy production. Trans. ASME, J. Heat Transfer 86, P. 247–252.
28. Chisholm, D., 1973. Pressure gradients due to friction during the flow of evaporating two-phase mixtures in smooth tubes and channels, Int. J. Heat Mass Transfer 16, P. 347–358.
29. Hart J., P. J. Hamerma and J. M. Fortuin, 1989,"Correlations Predicting Fractional Pressure Drop and Liquid Holdup During Horizontal Gas-Liquid Pipe Flow with a Small Liquid Holdup", Int. J. Multiphase Flow, Vol. 15, No. 6. P. 947-984.
30. Petalaz, N., Aziz, K., 1997. A mechanistic model for stabilized multiphase flow in pipes. Technical Report for Members of the Reservoir Simulation

Industrial Affiliates Program (SUPRI-B) and Horizontal Well Industrial Affiliates Program (SUPRI-HW), Stanford University, Palo Alto, CA.

31. Zhao, H.D, Lee, K.C., Freeston, D.H., 2000. Geothermal two-phase flow in horizontal pipes. In: Proceedings World Geothermal Congress, Kyushu-Tokyo, Japan, May 28–June 10, P. 3349–3353.

32. Brodkey R. S. and H. C. Hershey, Transport Phenomena, 2nd Printing, Mc Graw Hill, New York, 1989.

33. Andreussi P. and S. Zanelli, 1989," Down Annular and Annular –Mist Flow of Air Water Mixtures, Two Phase Momentum, Heat, and Mass Transfer in Chemical Process and Energy Engineering System, Int. Centre for Heat and Mass Transfer, Belgrade, Hemisphere Publishing Co., Washangton, Vol.1.

34.Sripattrapan S. and Wongwises S., 2008, Flow pattern, void fraction and pressure drop of two-phase air–water flow in a horizontal circular micro-channel

Experimental Thermal and Fluid Science, Volume 32, Issue 3, P. 748-760.

35. Wang S. and S.Nesic, 2003, On Coupling CO_2 Corrosion And Multiphase Flow Models, Corrosion 03631, paper No. 03631.

36. Knudsen, J. G. and D. L. Katz, 1958, Fluid Dynamics and Heat Transfer, Mc Graw Hill, New York.

37.Slaiman Q. J., M. Abu-Khader, and Basim O. Hasan, 2007, "Prediction of Heat Transfer Coefficient Based on Eddy Diffusivity Concept", Trans. IChemE, Part A, Chemical Engineering Research and Design, 85(A4): 455-464.

38. Welty, J. R., C. E. Wicks, and G. Rorrer, 2001, Fundamentals of Momentum, Heat, and Mass Transfer, 4th Edition, John Wiley and Sons, United States of America.

39.Dukler A., Fabre J., McQuillen J. and Vernon R., 1988, Gas-liquid flow at microgravity conditions: Flow patterns and their transitions." Int. J. Multiphase flow, Vol.14, No.4, pp. 389-400.

Nomenclature

A	Area, m^2
d	Pipe diameter, m
d_{hL}	Hydraulic diameter of liquid, m
f	Friction factor
h_L	Height of liquid layer, m
R	Pipe radius, m
Re	Reynolds number, ρdu/μ
Re_{sg}	Reynolds number based on gas superficial velocity
Re_{sL}	Reynolds number based on liquid superficial velocity
P	Pressure, N/m^2
$\dot{m}$	Mass flow rate, kg/s
S	Surface Area, m^2
Sh	Sherwood number
T	Temperature, ^oC
u	Velocity, m/s
u^*	Friction velocity, m/s
V	Volume, m^3
y	Distance from the wall, m
y^+	Dimensionless distance from the wall
y^+	Dimensionless distance from the wall
z	Axial distance, m
r	Radial distance, m
L_t	Thermal entrance length
Q	Volume flowrate, m^3/s
C_p	Specific heat, kJ/kg. ^oC
q''	Heat flux, J/m^2

Greek Letters

α	Thermal molecular diffusivity, m^2/s
δ	Thermal layer thickness, m
μ	Kinetic viscosity, kg/m. s
ν	Kinematic viscosity, m^2/s
ε	Void fraction
ρ	Density, kg/m^3
τ	Shear stress, N/m^2

Subscripts

b	Bulk
g	Gas
i	Interface
L	Liquid
TP	Two phase
w	Wall
hL	Hydraulic diameter of liquid
sL	Liquid superficial
sg	Gas superficial
t	Thermal
σ	Shear stress, N/m